Surface Microstructure Modification in Square Extruded Al-Nb Powder Composites by Shot Peening

2014 IOP Conf. Ser.: Mater. Sci. Eng. 63 012015

(http://iopscience.iop.org/1757-899X/63/1/012015)

IOP Conf. Series: Materials Science and Engineering **63** (2014) 012015 doi:10.1088/1757-899X/63/1/012015

Surface Microstructure Modification in Square Extruded Al-Nb Powder Composites by Shot Peening

Heinz-Günter Brokmeier[1, 3], Martina C. Avalos[2], Raúl E. Bolmaro[2], Emad Maawad[3]

[1]Institut für Werkstoffkunde und Werkstofftechnik, Technische Universität Clausthal, Agricolastr. 6, 38678 Claustahl-Zellerfeld, Germany.
[2]Instituto de Física Rosario-Facultad de Ciencias Exactas, Ingeniería y Agrumensura CONICET-UMR, Bv. 27 de Febrero 210 bis, (S2000EZP), Rosario, Argentina.
[3]Helmholtz-Zentrum Geesthacht (HZG-WPN), Notkestr. 85, 22607 Hamburg, Germany.
E-mail: heinz-guenter.brokmeier@tu-clausthal.de

Abstract. 75%Al-25%Nb powder composites, fabricated by square shape cold extrusion, were subject to shot peening treatment with full coverage. Shot peening results in a high number of intense local deformations, with a surface roughness in our case of about 16µm. Due to the high local deformation down to nano-scale surface grain refinement and strain accumulation was generated. Previous texture characterization was performed by neutron diffraction and laboratory X-rays (Cu K_α radiation). The first method took advantage of the high penetration power and averaging capabilities and the second method was further used taking advantage of the low penetration to characterize surface microstructure modification. Peak broadening, before and after shot peening, was analyzed by MAUD software and domain sizes and microstrains were calculated for both phases. Simultaneous EBSD and EDS scans, on 30 nm step sizes, were performed on a FESEM Quanta 200 + TSL-EDAX, showing the highly heterogeneous microstructure developed because of shot peening. Protrusions, due to particle impacts, are clearly seen on EBSD maps. Results mainly revealed that, for Al phase, domain sizes decrease, while microstrains and dislocation densities consistently increase after the materials have been subjected to SP. For Nb phase the visible effect of SP is an increment of microstrains, and related dislocation densities, but keeping the domain sizes almost constant.

1. Introduction

Metal composite materials made of powder precursors usually present serious detriment on their mechanical properties due to many defects of fabrication (pores, oxide phases, stress incompatibility, etc.). By pre-compacting powder mixtures and extruding the pre-form, a close contact between particles and microalloying effect can be achieved. Combining advantageous characteristics of different materials by making a composite summing them up on the right proportion is a typical strategy. However the surfaces may present pores and defects that conspire against the expected properties. This can result in failures due to, for example, fatigue fracture, fretting fatigue, wear and corrosion which are very sensitive to the structure and properties of the material surface. Thus, surface nanocrystallization is expected to greatly enhance the surface property without changing the chemical compositions and shape of materials [1,2].

Surface nanocrystallization can be developed by applying locally severe plastic deformation by means of mechanical surface treatments such as shot peening and ball-burnishing [3].

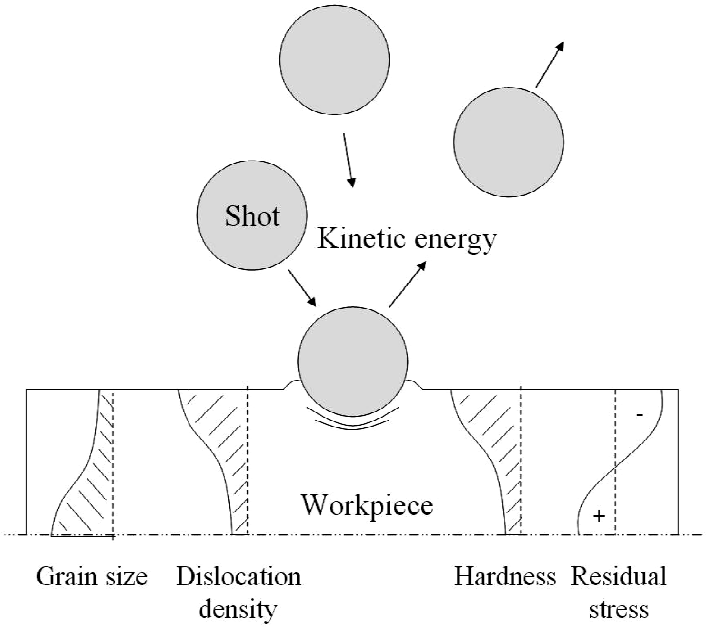

Fig. 1: Surface modification by shot peening

This lead to intensive changes on surface microstructure [4], crystallographic texture [5] and stress state [6]. Shot peening (SP), shown schematically in Fig. 1, is a process used to produce a compressive residual stress layer and modify mechanical properties of metals. The changes in the surface state due to SP are, for example, changes of the residual stresses, microstructures, hardness by work-hardening, surface roughness, cracks, crystallographic texture and dislocation density [7]. It entails impacting a surface with shooting particles (round metallic, glass or ceramic) with a kinetic energy sufficient to create plastic deformation, each shot that strikes the material acts as a tiny peening hammer, imparting to the surface a small indentation or dimple. To create the dimple, the surface of the material must yield in tension. Below the surface, the material tries to restore its original shape, thereby producing below the dimple a hemisphere of cold-worked material highly stressed in compression. Many process parameters are of importance for the surface characteristics after SP.

Some articles have been published concerning cold and hot extruded and cold rolled textural evolution of Al-Nb composites [8-10] as well as their mechanical behaviors at room and elevated temperatures [11]. Of key interest was the texture change during annealing and phase transition [12]. However, there is little information about the influence of SP process on the surface characteristics of that composite. Thus, this work aimed to study the changes in the surface microstructure and the local texture after applying SP on 75%Al-25%Nb powder composites by means of EBSD, X-ray and neutron diffraction.

2. Experiment description

The investigated material is a square extruded 75%Al-25%Nb powder composite. The composite was prepared from elementary irregular shape Al powder with a purity of 99.94% (grain size <100 μm) and from elementary Nb powder (purity 99.90%, grain size 100-300 μm, irregular shape). Powder metallurgy has the great advantage that materials with very different melting temperatures (660°C for Al and 2400°C for Nb) can be pressed together to obtain compact samples. The powders were mixed in a turbulent mixer for about 1 h under argon atmosphere. Thereafter the powder mixture was pre-compacted to cylinders of 50 mm

of radius by uniaxial pressure to about 80% ideal density. Cold extrusion from cylinder to rectangular shape of 5x20 mm² was performed to a deformation degree of 96%.
Part of this extruded bar was cut to analyze the bulk texture by neutron diffraction. The measurement was carried out at the texture diffractometer TEX2@FRG-1/Geesthacht [13]. A neutron wavelength of 1.618Å was used to measure three pole figures for each phase. Due to overlapping of Al (111) with Nb (110) the strongest reflection for each phase could not be measured. Thus Al (200), (220) and (311) as well as Nb (200), (210) and (310) were used. Due to the comparably low percentage of Nb these measurements are very time consuming. The quantitative texture was calculated by the iterative series expansion method, ISEM after Bunge, to obtain complete ODF (ODF-Orientation Distribution Function).
Shot peening was performed with an injector type machine using spherically conditioned cut wire SCCW14 (0.36 mm average shot size). Specimens were shot peened to full coverage using Almen intensity of 0.2 mm A.
Surface roughness was determined by means of an electronic contact (stylus) profilometer instrument (Perpethometer). For Ra a roughness of 3.63 μm was obtained. Ra is the arithmetic average of the absolute values of the roughness profile ordinates, also known as Arithmetic Average (AA), or Center Line Average (CLA). The average roughness is the area between the roughness profile and its mean line. Rz is the absolute average value of the five highest peaks and the five lowest valleys over the evaluation length determined to RZ=16.37 μm. For statistical reasons the roughness measurement was repeated three times.
After SP the texture was also measured on the peened area to check possible surface texture changes. We used laboratory x-ray radiation to guarantee interactions only with the surface modified region. A Panalytical X-pert MPD Cu Kα equipment was used. Results were post-processed by popLA, current Windows based texture software. Diffractograms with very low angle divergence were taken for microstructural determination. Machine broadening was characterized by measuring, with the same experimental setup, a LaB_6 NIST powder standard.
For EBSD characterization the main problem comes from the different characteristics of both phases and different reactions under polishing. Al phase tends to be more easily attacked by any chemical and gets ground easier than Nb. A very careful polishing was performed by diamond suspension (9, 6, 3 and 1 μm) and later on 30 minutes of vibratory polishing was performed with 0.05 μm colloidal silica suspension. The scans were performed on a FEI Quanta 200 FEG SEM equipped with an EBSD EDAX detector + TSL-EDAX analysis software. The scanning mode used simultaneous detection with EDS EDAX detector to allow better choice of the phase.

3. Results and Discussion

3.1. Texture characterization

The bulk texture of the composite shows the well-known metal textures of the two components, resulting from plain strain deformation (rolling, bar extrusion or channel die). Fig. 2 shows the $\varphi_2 = 45°$ ODF sections of Al and Nb. In Al, one can see the copper and brass components dominating the texture together with the S-component, typical for Al-deformation. The maximum orientation strength was 5.8 m.r.d.. Compared to pure Al this was much lower because of the co-deformation with Nb. Niobium shows a dominating rotated cube component, an α-fiber distribution with continuous decrease of orientations from $\varphi_1=0°/\Phi= 0°$ to $\varphi_1 =0°/ \Phi =90°$ and a weaker $(111)[0\bar{1}1]$ component.
Figures 3 a-b show the starting surface texture (before SP) which resembles the neutron measured textures, with lower strengths and minor component shifts due probably to friction on the surface of the sample and the die during extrusion, and to the lower averaging capabilities of low energy x-rays. After SP the sample was re-measured on the peened surface by laboratory X-rays. The surface texture (Figures 3 c-d) changed to almost random for the Al phase and to a low strength cylindrically symmetric texture for Nb phase.

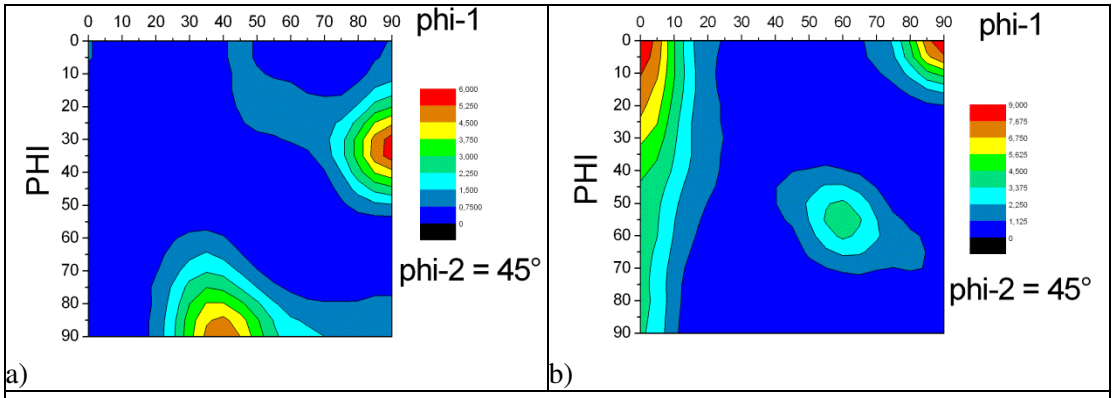

Fig. 2: ODF section of Al75%-Nb25% after 96% cold square extrusion.
a) Al phase, b) Nb phase

Figures 4 a-b show the φ_2=45° sections, analogous to the ones obtained by neutron diffraction, for the as extruded (AE) sample. Sections look pretty much alike with the differences probably stemming from surface heterogeneities.

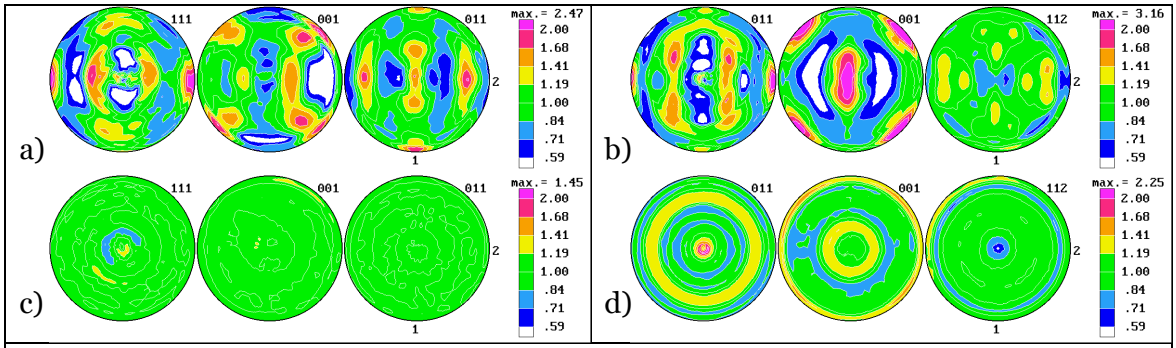

Figure 3. Starting surface texture,before shot peening. a) Al phase. (111), (001) and (011) Pole Figures b) Nb phase. (011), (001) and (112) Pole Figures. Idem after shot peening c) Al phase d) Nb phase

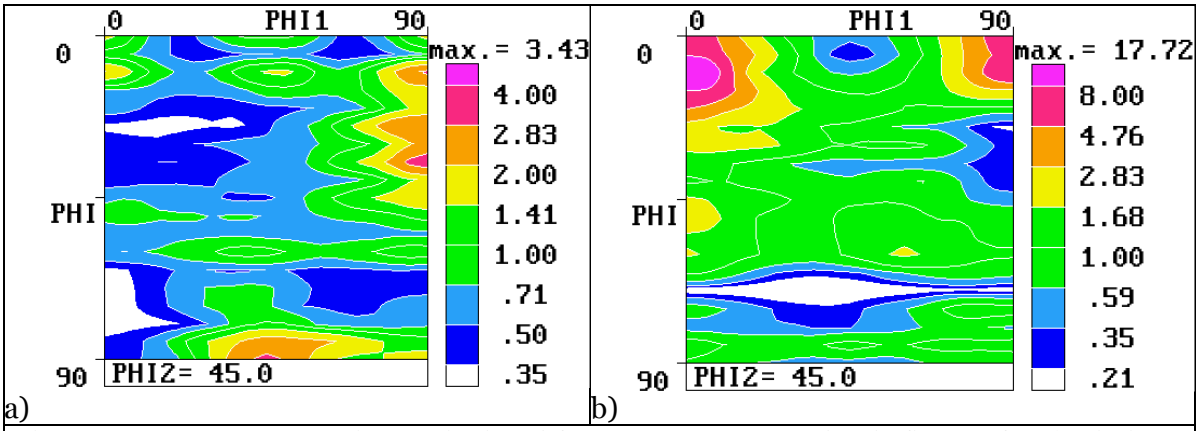

Figure 4. φ_2=45° ODF sections calculated from X-ray measured pole figures for a) Al phase b) Nb phase.

3.2. Microstructural characterization by peak broadening analysis

Further understanding of the deformation process, through X-ray analysis, can be achieved by processing the diffractograms with the purpose of calculating domain sizes and dislocation densities from peak broadening effects. X-ray diffraction measurements were performed on the as extruded material and on the shot peened surface. The diffractograms were analyzed by two techniques to characterize peak broadening and to calculate domains sizes (D) and micro-strains in both phases. One of the techniques consists on analyzing the diffractograms by Rietveld fit as implemented on Maud software. Volume fraction and texture can be calculated and micromechanical characterization can be achieved as described in Ischia et al. [14] and Lutterotti and Bortolotti [15]. A previous characterization of machine peak broadening was performed by measuring a LaB_6 NIST powder standard sample.

The other technique is the one known as the Williamson-Hall method [16], modified by Ungár [17, 18] and Warren [19] (MW-H). All peaks are fit with a Pseudo-Voight function and integral peak broadening is calculated and, after subtraction of the instrumental integral peak broadening, the values are fit by the equation:

$$\frac{Breathcos\theta}{\lambda} - \beta W_g = \frac{1}{d} + \left(\frac{\pi M^2 b^2}{2}\right)\rho^{1/2}K^2C \qquad (1)$$

where d is the diffraction domain size, λ is the wavelength of the radiation, β is the stacking fault density, W_g are the Warren constants related to the stacking faults, ρ is the dislocation density, b is the Burgers vector, M is a constant related to the cut-off radius of dislocations (which is smaller for more compact arrays), C are the average contrast factors of dislocations and K=2 sin (θ)/λ.

Figure 5 a-b) shows results from MAUD analysis and from W-H model. For Al phase, as expected, domain sizes decrease and microstrains and dislocation densities consistently increase, as determined by both methods, after the materials have been subjected to SP. For Nb phase the visible effect of SP is an increment of microstrains, and related dislocation densities, but keeping the domain sizes almost constant. These results can be rationalized by assuming that dislocation densities produced by SP on Nb are of a more loose character than the ones stored on Al phase, where they promote thicker dislocation arrays and smaller domains.

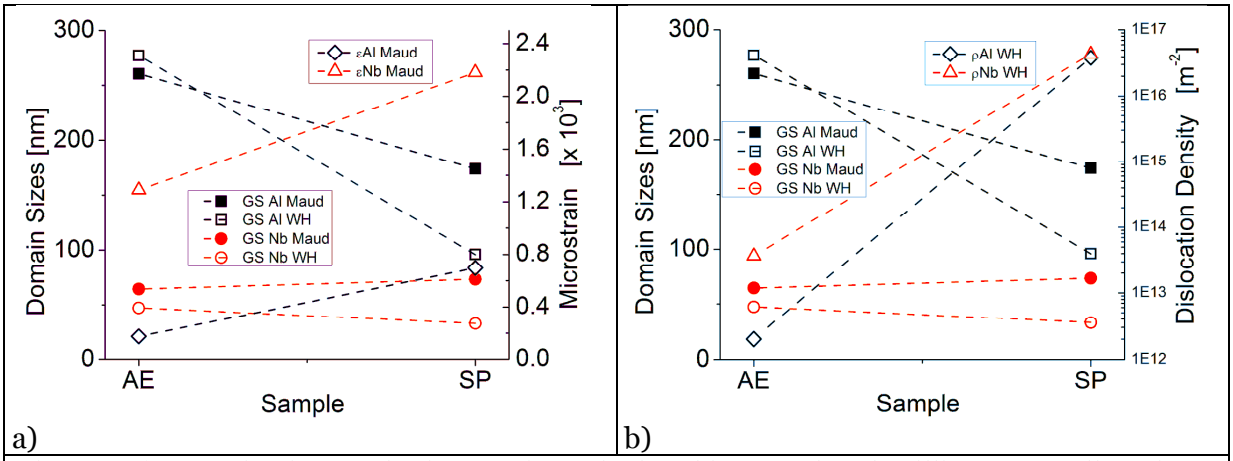

Figure 5 a) Domain sizes and microstrains calculated by Maud and Williamson-Hall analyses b) Same domain size results and dislocation densities from W-H model.

3.3. EBSD results

The extruded material shows a typical wavy microstructure of a metal matrix composite. During co-deformation the softer Al-matrix flows around the larger Nb particles. This results in a grain refinement of the Al particles during cold extrusion, meaning the Al undergos a higher deformation than Nb. The Nb "lenses" show an elongation in extrusion direction. Larger particles show more clear the Nb deformation. Average Grain Size distributions were calculated, as area fraction and with a relative misorientation of 1º defining a closed grain. A close to Gaussian distribution (with grain size in logarithmic scale) for Al phase and a fast growing distribution at large grain sizes for Nb phase are shown on Fig. 6. Even at the smallest misorientation of 1º, the average size of the grains is about one order of magnitude larger than the one determined by X-ray analysis for Al phase and 3 orders larger for the Nb. That comes from the relatively low resolution of EBSD, both in space and orientation angle, with respect to X-rays. The data has actually the opposite behavior with Nb grains larger than Al grains by EBSD determination, while domain sizes are larger for Al than for Nb.

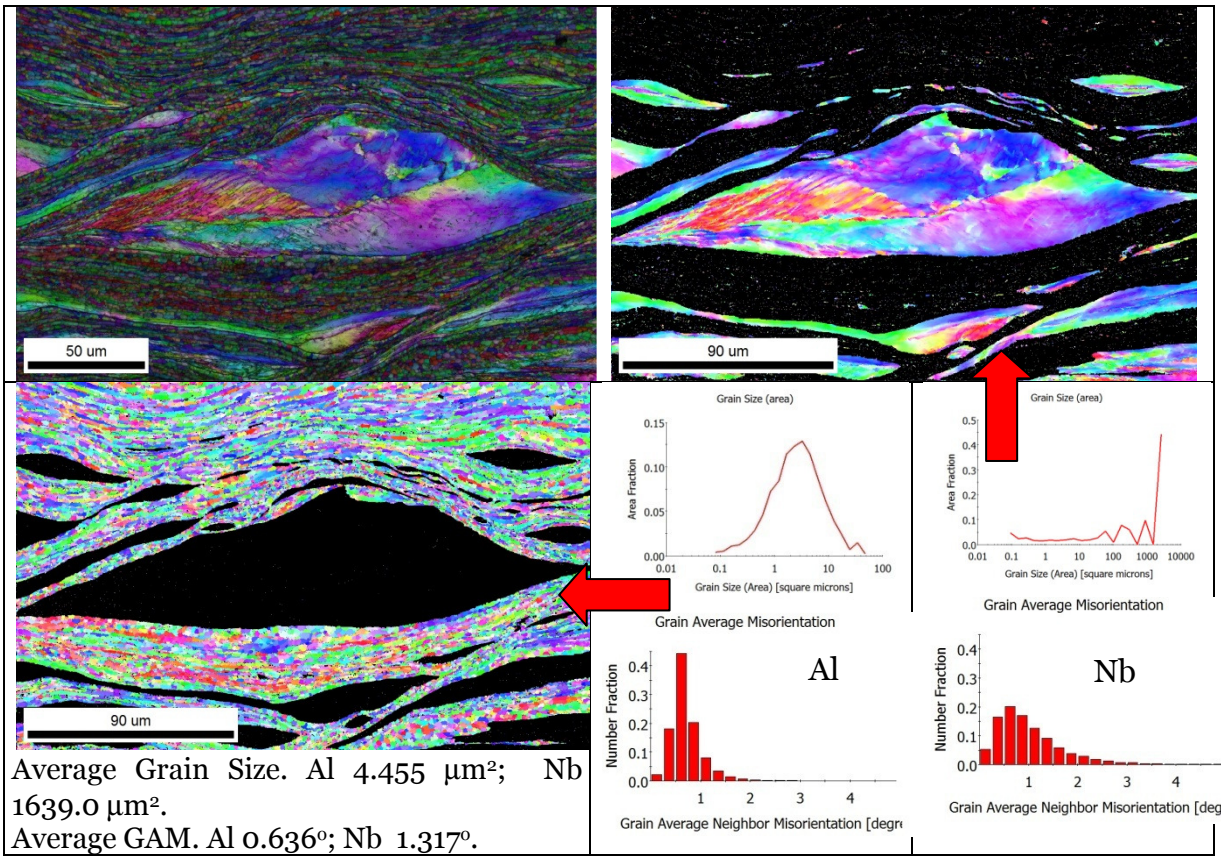

Average Grain Size. Al 4.455 μm²; Nb 1639.0 μm².
Average GAM. Al 0.636º; Nb 1.317º.

Fig. 6: Microstructure of cold square extruded 75%Al-25%Nb determined by EBSD. Step size=100 nm.

Grain Average Misorientation distributions (with the kernel limited to the 1st neighbor) were calculated for both phases. Somehow surprisingly, the Al GAM distribution shows a smaller standard deviation (less spread) and smaller average than the Nb GAM distribution. The deformation process on the Al phase is reflected as very small sub-grains but with very small internal misorientations. The Nb phase, which looks as larger grains, shows a larger internal misorientation reflected on the calculated GAM.

Figure 7 shows an EBSD scan on the shot peened border. Round polycrystalline particles, mostly made of Nb phase, surrounded by fine grained Al phase, are formed due to the

impacts. Both phases appear as been refined, in contraposition with the diffraction analysis results, by which the Al phase domain sizes diminish appreciably while Nb phase keeps almost the same domain size.
Figure 8 shows another border scan, where formation of dimples and round polycrystalline particles is also evident. Misorientation and grain size (area fraction) distributions are shown separately for Al and Nb phases. By comparison with the values on the central bulk of the sample (Fig. 5 and related data), we can see that EBSD can detect only a minor decrease on grain sizes for both Al and Nb phases. GAM calculated for the Al shows a slight increment of approximately 15% while Nb shows a decrease of 5%. Both values might be only representative of statistic variations.
Reducing the region of interest to a very narrow layer of approximately 80 μm from the surface the same calculations provide average grain sizes of 4.34 μm^2/192 μm^2 and GAMs of 0.518°/0.803° for Al and Nb respectively. The reduction on grain sizes together with a decrement on GAM for Nb is noticeable but the values are still far from the expected taking in account X-ray calculations.

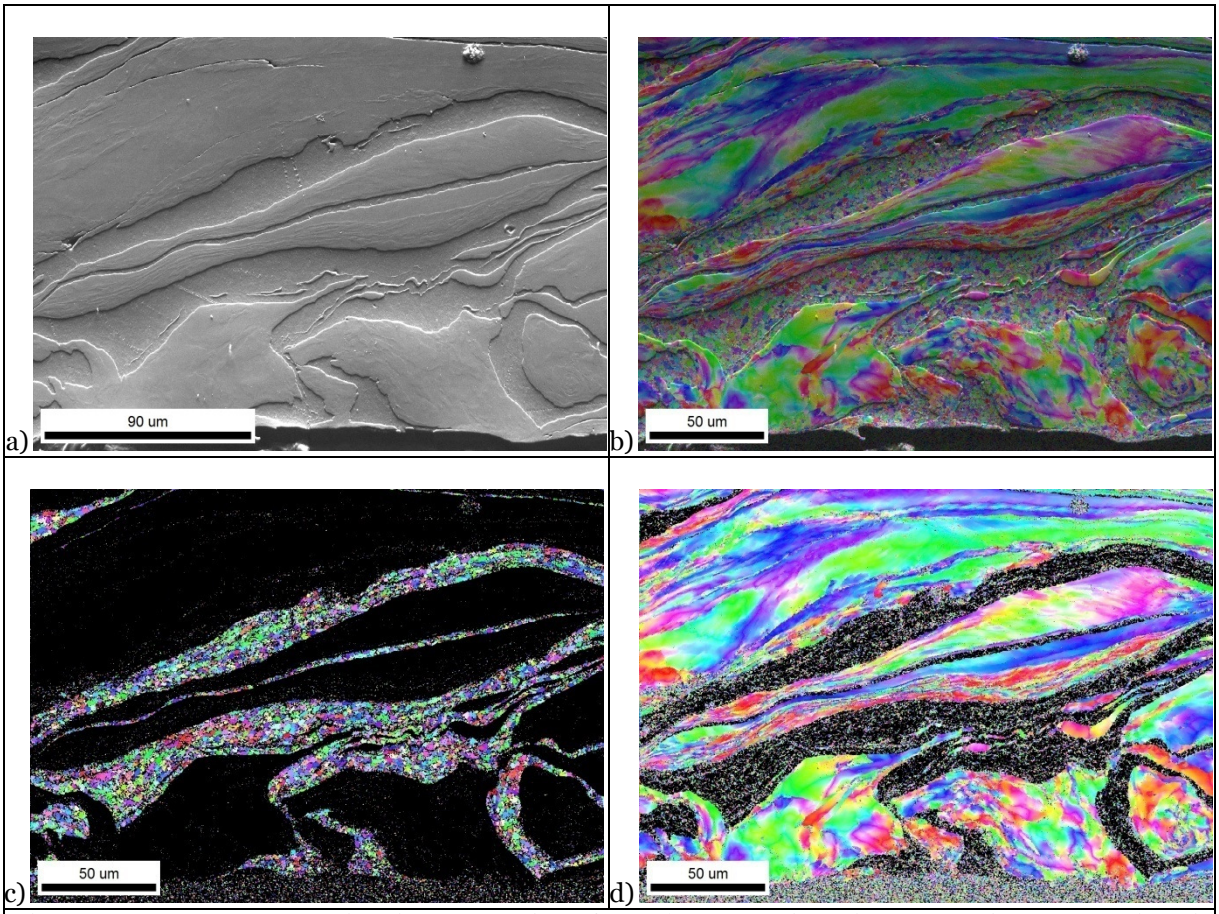

Figure 7. EBSD scans on the shot peened surface. a) Forward Back Scattered Detector signal. b) Scan with 100 nm step size. c) Al phase partition. d) Nb phase partition.

4. Discussion and conclusions

Mixing two phases with quite apart mechanical and thermo-dynamical properties allows the development of grains sizes and dislocation arrays that may look somehow contradictory when tools appropriate for slightly different scales are used. Moreover, extrusion and SP are two quite different methods of imparting plastic deformation. Extrusion is a low rate, fairly

homogeneous and monotonous strain imposing mode, while shot peening is a high strain rate, highly heterogeneous and strain redundant way of enforcing plastic deformation. Low and high strain rate deformations differ quite a lot on the active mechanisms for plastic deformation and consequently on the kind and quantity of stored defects.

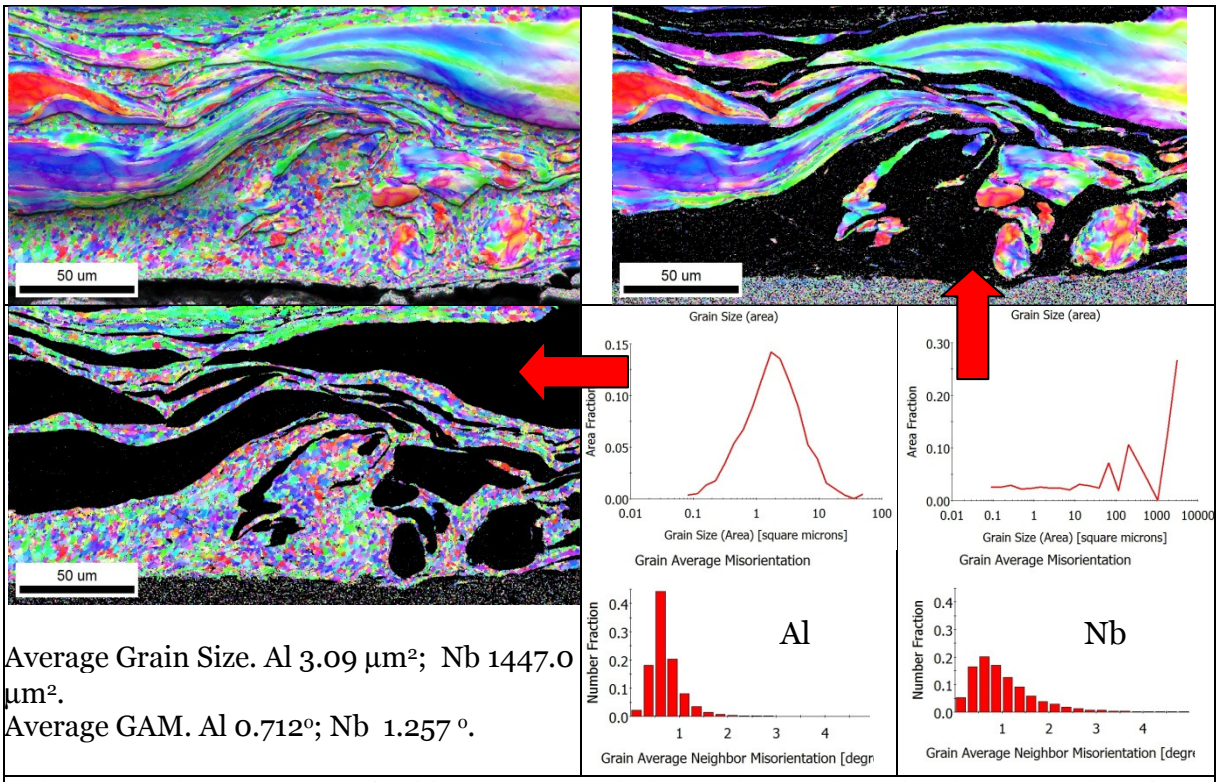

Average Grain Size. Al 3.09 μm²; Nb 1447.0 μm².
Average GAM. Al 0.712º; Nb 1.257 º.

Figure 8: Microstructure of cold square extruded 75%Al-25%Nbon the shot peened surface determined by EBSD. Step size 100 nm. EBSD scans on the shot peened surface. a) Forward Back Scattered Detector signal. b) Scan with 100 nm step size. c) Al phase partition. d) Nb phase partition.

Even well-established methods of analysis on property contrasting poly-phase materials can be deceiving. Regular high resolution EBSD is helpful on visualizing microscopic effects but, despite its paramount abilities for detecting micro-texture features, the smallest nanoscopic details claim for a finer probe. The step size used for the scans (100 nm) is not the lowest available on this technique (20-30 nm) but using a smaller one would prohibitively increase scanning times or diminish scanning areas, worsening statistic. Laboratory X-rays, together with proper analysis techniques, can shed light on those finer features and help on the understanding of the whole picture. A careful study, perhaps with Transmission Electron Microscopy and/or high energy synchrotron radiation may allow a better and detailed determination of the microstructures developed in each phase.

Acknowledgements
This work was supported by ANPCyT - Argentina and the International Collaboration CONICET-DFG-Germany (BR961/6-1).

References

[1] Bagheri Fard S and Guagliano M 2009 *Frattura ed Integrità Strutturale* **7** 3
[2] Erb U, EI-Sherik A, Palumbo G and Aust K 1993 *Nanostruct. Mater.* **2** 383.
[3] Baiker S (Ed.), **Shot Peening, A Dynamic Application and Its Future,** First ed., Switzerland, 2006.
[4] Xie L, Wang L, Jiang C and Lu W 2014 *Surf. Coat. Technol.* **244** 69.
[5] Maawad E, Brokmeier H-G and Wagner L 2010 *Solid State Phenomena* **160** 141.
[6] Menig R, Pintschovius L, Schulze V and Voehringer O 2001 *Scripta Mater.* **45**5 977.
[7] Schulze V, in: *Proc. of the 8th Int. Conference on Shot Peening,* L Wagner (Ed.) Garmisch–Partenkirchen, Germany, 2002, pp 145.
[8] Chen L Q and Kanetake N 2003 *Textures and Microstructures* **35** 273.
[9] Chen L Q and Kanetake 2002 *Materials Science Forum* **408-412** 1765.
[10] Schnieber R and Brokmeier H-G 1999 *Materials Science Forum* **321-324** 631.
[11] Chen L Q and Kanetake 2004 *Mater. Sci. Eng*. **A 367** 295.
[12] Schnieber R, Bunge H J and Brokmeier H-G 1999, in *Proc. of ICOTOM 12*, J.A. Szpunar (Ed.) NRC Research Press, Ottawa, 1999, pp 1172.
[13] Brokmeier H-G, Zink, U, Schnieber, R, and Witassek, B. 1998 *Materials Science Forum* **273-275** 277.
[14] Ischia G, Wenk H-R, Lutterotti L and Berberich F. 2005 *J. Appl. Cryst.* **38(2)** 377.
[15] Lutterotti L and Bortolotti M 2003 *IUCr: Compcomm Newsletter* **1** 43.
[16] Williamson G K and Hall W H 1953 *Acta Metallurgica* **1**, 22.
[17] Ungár T, Gubicza J, Hanák P and Alexandrov A 2001 *Mater. Sci. Eng*. **A 319–321** 274.
[18] Warren B E 1959 Progress in Metal Physics **8** 147.
[19] Ungár T, Dragomir I C, Révész Á and Borbély A 1999 *J. Appl. Cryst.* **32** 992.